Massflux Budgets of Shallow Cumulus Clouds[1]

Stephan R. de Roode

Christopher S. Bretherton

Department of Atmospheric Sciences, University of Washinton, Seattle, WA, USA

Submitted to the *Journal of the Atmospheric Sciences*, September 14, 2001

[1]Corresponding author address: Stephan R. de Roode, Institute for Marine and Atmospheric Research Utrecht (IMAU), Princetonplein 5, 3584 CC Utrecht, The Netherlands. Email: roode@phys.uu.nl

Abstract

The vertical transport by shallow nonprecipitating cumulus clouds of conserved variables, such as the total specific humidity or the liquid water potential temperature, can be well modeled by the massflux approach, in which the cloud field is represented by a top-hat distribution of clouds and its environment. The budget of the massflux is presented and is compared with the vertical velocity variance budget. The massflux budget is computed by conditionally sampling the prognostic vertical velocity equation by means of a Large-Eddy Simulation of shallow cumulus clouds. The model initialization is based on observations made during BOMEX. Several different sampling criteria are applied. The presence of liquid water is used to select clouds, whereas additional criteria are applied to sample cloud updraft, downdraft and core properties. The massflux and vertical velocity variance budgets appear to be qualitatively similar. The massflux is driven by buoyancy in the lower part of the cloud layer, whereas turbulent transport is important in generating massflux in the upper part of the cloud layer. Pressure and subgrid-scale effects typically act to dissipate massflux. The massflux approach is verified for non-conserved variables. The virtual potential temperature flux and the vertical velocity variance according to the the top-hat approximation do not correspond very well to the Reynolds-averaged turbulent flux. The top-hat structure for the virtual potential temperature is degraded by lateral mixing and the subsequent

evaporative cooling of cloud droplets which support the development of negatively buoyant cloud downdrafts. Cloudy downdrafts occupy about 20% of the total cloud area in the upper part of the cumulus layer, and are the cause that the vertical velocity variance is not well represented by the massflux approach, either.

1. Introduction

The parameterization of vertical transport due to cumulus clouds is often performed by a massflux approach (Asai and Kasahara, 1967; Arakawa and Schubert, 1974; Tiedtke, 1989). In such schemes it is assumed that the cumulus cloud field can be well represented by a top-hat distribution. This decomposition requires a set of two separate prognostic equations that describe the (thermo-) dynamical evolution of the clouds, and the surrounding environment, respectively:

$$\frac{\partial \sigma \psi_c}{\partial t} = -\frac{\partial M_c \psi_c}{\partial z} + E\psi_e - D\psi_c + \sigma S_{\psi,c}, \tag{1}$$

$$\frac{\partial (1-\sigma) \psi_e}{\partial t} = \frac{\partial M_c \psi_e}{\partial z} - E\psi_e + D\psi_c + (1-\sigma) S_{\psi,e}, \tag{2}$$

with ψ an arbitrary conserved variable, M_c the convective massflux, t the time, z the height above the surface, and the subscripts $'c'$ and $'e'$ indicate the cloud and environmental value, respectively. Diabatic processes such as precipitation or radiation can be included in the source function S_ψ. These two equations both include an entrainment (E) and a detrainment (D) term that represent the effect of lateral mixing of mass at the cloud interface (Stommel, 1947; Arakawa and Schubert, 1974; Tiedtke, 1989; Siebesma and Holtslag, 1996). This parameterization of the net lateral exchange mirrors the idea that if the velocity at the cloud boundary is pointed cloud inward, air properties of the environment are entrained by the cloud, and vice versa.

The prognostic equations (1) and (2) include 4 unknowns that need to be parameterized: σ, M_c, E, and D. In the ECMWF model, for example, the fractional,

or normalized entrainment ($\epsilon = E/M_c$) and detrainment rates ($\delta = D/M_c$) are simply prescribed (Tiedtke, 1989). These values for the lateral mixing rates can be based on observations (Nitta, 1975; Raga et al., 1990) or results from large eddy simulation (LES) studies of shallow cumuli (Siebesma and Cuijpers, 1995; Grant and Brown, 1999; Stevens and Co-Authors, 2000). Given algorithms for E and D, $M_c(z)$ is found from the continuity equation for mass

$$\frac{\partial M_c}{\partial z} = -\rho \frac{\partial \sigma}{\partial t} + E - D, \tag{3}$$

such that the system can be closed by either diagnosing or predicting the cloud fraction σ. To simplify the governing set of equations, it is usually assumed in cumulus parametrizations that $\sigma << 1$. In that case the l.h.s. of (1) can be dropped, in (2) $1 - \sigma$ can be replaced by 1, and $\rho \partial \sigma / \partial t$ can be deleted in (3). Note that $\sigma(z,t)$ is only used for the calculation of radiative fluxes, where one must also consider vertical cloud overlap. LES-based studies of shallow cumuli have shown that with suitable entrainment and detrainment rates, a massflux decomposition can represent quite well the simulated vertical fluxes of conserved thermodynamic variables (Siebesma and Cuijpers, 1995).

Some massflux-based cumulus parameterizations also prognose an updraft vertical velocity using an equation similar to (1) (Asai and Kasahara, 1967; Holton, 1973; Cotton, 1975), with source terms representing updraft buoyancy and vertical pressure gradient forces. This vertical velocity permits consideration of convection that penetrates above its level of neutral buoyancy, can be used in microphysical calculations, and the ratio of massflux to vertical velocity can be used to diagnose

cloud fraction. In view of the utility of a vertical velocity equation, our main goal in this paper is to investigate how well the massflux decomposition can represent the vertical velocities and vertical velocity variance budget in LES of shallow cumuli.

In section 2, we derive the conditionally sampled budget equation for the massflux. In section 3, we summarize the LES of trade cumuli during BOMEX (the Barbados Oceanographic and Meteorological EXperiment in June 1969) which we use to analyze these budgets. In section 4, we present the conditionally sampled massflux budgets for various sampling criteria defining the active clouds, and compare them with Reynolds-averaged variance budgets. In section 5 we analyze reasons for the poor performance of the tophat (massflux) approximation in explaining the buoyancy and vertical velocity budgets. Conclusions follow in section 6.

2. Derivation of the budget equations for the vertical velocity and the convective massflux

a. Governing equations

In our simulations and analyses, we use the Boussinesq equations and their LES implementation. The conservation equations for an arbitrary conserved variable ψ and the Boussinesq form of the momentum equation read, respectively,

$$\frac{\partial \psi}{\partial t} + u_j \frac{\partial \psi}{\partial x_j} = S_\psi, \tag{4}$$

$$\frac{\partial u_i}{\partial t} + u_j \frac{\partial u_i}{\partial x_j} = \frac{g}{\theta_0}(\theta_v - \theta_0)\delta_{i3} - \frac{1}{\rho}\frac{\partial p}{\partial x_i}. \tag{5}$$

The conserved variable ψ can represent, for example, the total water specific humidity q_t or the liquid water potential temperature θ_l. S_ψ is a source term that can represent processes like radiation or precipitation. The velocity components $u_i = (u, v, w)$ are the components in $x_i = (x, y, z)$ directions, respectively, p is pressure, t is the time, g the gravitational acceleration, θ_v the virtual potential temperature, θ_0 the reference state potential temperature, and δ_{ij} the Kronecker delta.

b. Definitions

The conditionally sampled mean value $[\psi]_s$ of any arbitrary variable ψ is defined as

$$[\psi]_s = \frac{\int_A I_s \psi dA}{\int_A I_s dA}, \tag{6}$$

where the integration is performed over a horizontal plane at height z and I_s is an indicator function. $I_s = 1$ if a sampling criterion is met, and $I_s = 0$ otherwise. In the LES model the integrals are evaluated by a summation over discrete grid points (Schumann and Moeng, 1991). To determine properties of the cumulus clouds only, one usually samples on the presence of liquid water (q), although several other criteria are sometimes added. For instance, the cloud core is defined as the part of the cloud that has both an upward vertical velocity and a positive virtual potential temperature excess. The sampling criteria that have been applied

are summarized in Table 1. The sampled area fraction σ_s is defined as

$$\sigma_s = \frac{\int_A I_s dA}{\int_A dA}. \tag{7}$$

For a two-stream approximation we can define the fraction of the environment σ_e as

$$\sigma_e = 1 - \sigma_s. \tag{8}$$

By this definition the environment represents the area fraction of all points where the applied sampling criteria are not satisfied. If the sampling operator is moved inside a derivative, two additional terms arise due to the chain rule of differentiation and the application of Leibniz' rule (Young, 1988). The vertical advection term, for example, is then given by

$$\left[\frac{\partial w^2}{\partial z}\right]_s = \frac{\partial [w^2]_s}{\partial z} + \frac{[w^2]_s}{\sigma_s}\frac{\partial \sigma_s}{\partial z} + \left\{\frac{\partial w^2}{\partial z}\right\}_{b,s}, \tag{9}$$

where we used the notation $_b$ to indicate the net effect of the boundary terms which follow from Leibniz' rule. To calculate the term in curly brackets one needs to track the evolution of the cloud boundaries. However, one can avoid this laborous exercise if one calculates the other three terms in (9). In the remainder of the paper the square brackets that indicate the conditionally sampled mean are, for notational convenience, replaced by the subscripts '$_s$' or '$_e$' except when the operator is applied on a derivative. The slab-mean value (indicated by an overbar) of $\overline{\psi}$ is given by

$$\overline{\psi} = \sigma_s \psi_s + (1 - \sigma_s)\psi_e. \tag{10}$$

We define the massflux as

$$M_c \equiv \sigma_s w_s = \sigma_s(1-\sigma_s)(w_s - w_e), \tag{11}$$

which has, for convenience, units ms^{-1}. The Reynolds-averaged covariance $\overline{w'\psi'}$ is related to massflux variables as

$$\overline{w'\psi'} = \sigma_s(1-\sigma_s)(w_s-w_e)(\psi_s-\psi_e) + \sigma_s\overline{w'\psi'}^s + (1-\sigma_s)\overline{w'\psi'}^e, \tag{12}$$

where the overbars indexed '^{s}' and '^{e}' indicate the so-called sub-plume terms, which are due to the contributions of perturbations with respect to the conditionally sampled mean (Siebesma and Cuijpers, 1995).

c. The prognostic massflux equation

Conditionally sampling Eq. (5) gives

$$\left[\frac{\partial w}{\partial t}\right]_s = [S_w]_s, \tag{13}$$

where

$$S_w = \frac{g}{\theta_0}(\theta_v - \theta_0) - \frac{\partial w^2}{\partial z} - \frac{\partial u_h w}{\partial x_h} - \frac{1}{\rho}\frac{\partial p}{\partial z}, \tag{14}$$

and $u_h = (u, v)$ and $\partial x_h = (\partial x, \partial y)$. An identical equation as (13) can be written for the environment simply by replacing the subscript '$_s$' by '$_e$'. If we multiply Eq. (13) with σ_s and subtract the conditionally sampled prognostic velocity equation for the environment multiplied with a factor $(1-\sigma_s)$, we obtain

$$\sigma_s(1-\sigma_s)\left(\left[\frac{\partial w}{\partial t}\right]_s - \left[\frac{\partial w}{\partial t}\right]_e\right) = -\sigma_s(1-\sigma_s)\left([S_w]_s - [S_w]_e\right). \tag{15}$$

The time derivative in Eq. (15) can be rewritten as the tendency of the massflux

$$\sigma_s(1-\sigma_s)\left(\left[\frac{\partial w}{\partial t}\right]_s-\left[\frac{\partial w}{\partial t}\right]_e\right)=$$
$$(1-\sigma_s)\frac{\partial \sigma_s w_s}{\partial t}+(1-\sigma_s)w_b\frac{\partial \sigma_s}{\partial t}-\sigma_s\frac{\partial(1-\sigma_s)w_e}{\partial t}+\sigma_s w_b\frac{\partial \sigma_s}{\partial t}= \quad (16)$$
$$\frac{\partial M_c}{\partial t}+\sigma_s(1-\sigma_s)\left(\left\{\frac{\partial w}{\partial t}\right\}_{b,s}-\left\{\frac{\partial w}{\partial t}\right\}_{b,e}\right),$$

where we used (9) and (11).

3. Experimental set-up of the simulation

a. Large-eddy simulation of the BOMEX case

The large-simulation has been performed with the IMAU/KNMI model (Cuijpers, 1994; Siebesma and Cuijpers, 1995; VanZanten, 2000). To solve the basic governing equations (4) and (5) numerically one needs to filter them in order to distinguish between resolved and subgrid motions. The filtered prognostic equations for the resolved part of ψ and the velocity u_i read, respectively

$$\frac{\partial \psi}{\partial t}=-\frac{\partial u_j\psi}{\partial x_j}-\frac{\partial \overline{u_j''\psi''}}{\partial x_j}+S_\psi, \quad (17)$$

$$\frac{\partial u_i}{\partial t}=\frac{g}{\theta_0}(\theta_v-\theta_0)\delta_{i3}-\frac{\partial u_i u_j}{\partial x_j}-\frac{\partial \pi}{\partial x_i}-\frac{\partial \tau_{ij}}{\partial x_j}, \quad (18)$$

where $\overline{u_j''\psi''}$ and τ_{ij} are the subgrid flux terms and π is the modified pressure (Deardorff, 1973). In the LES model the subgrid fluxes are expressed as the product of an eddy viscosity K_m or eddy diffusivity K_ψ and the local gradient of the resolved variable:

$$\overline{u_j''\psi''}=-K_\psi\frac{\partial \psi}{\partial x_j}, \quad (19)$$

$$\tau_{ij} = -K_m(\frac{\partial u_i}{\partial x_j} + \frac{\partial u_j}{\partial x_i}). \tag{20}$$

The simulation was done with a central-difference scheme (64 x 64 x 75 points). The horizontal and vertical grid spacings were 100 m and 40 m, respectively.

The initialization was based on the BOMEX field experiment. We performed a simulation of 6 hours, and used the results of the last 4 hours for our analysis by averaging over all output fields during this time period. Since only a few clouds penetrate the inversion layer above 1500 m, the statistics in this layer are very poor and are therefore not discussed. The initialization and large-scale forcings are described in detail by Siebesma and Cuijpers (1995) and a follow-up study by the participants of the GEWEX (Global Water and Energy Experiment) Cloud Systems Study Working Group 1 (Siebesma and Co-Authors, 2001). The mean virtual potential temperature and liquid water content after 2 hours of simulation are shown in Figure 2.

b. Analysis of massflux and Reynolds-averaged equations

De Roode et al. (2000) showed that the sum of the lateral mixing rates, $E + D$, can be interpreted as an inverse dissipation time scale. They came to this conclusion after combining Eqs. (1) and (2) to rewrite them into a single prognostic variance

equation

$$\frac{\partial \sigma(1-\sigma)(\psi_u-\psi_d)^2}{\partial t} = -2M_c(\psi_u-\psi_d)\frac{\partial \overline{\psi}}{\partial z} - \frac{\partial (1-2\sigma)M_c(\psi_u-\psi_d)^2}{\partial z} - (E+D)(\psi_u-\psi_d)^2. \tag{21}$$

They compared this budget equation with the prognostic Reynolds-averaged variance equation, which reads,

$$\frac{\partial \overline{\psi'^2}}{\partial t} = -2\overline{w'\psi'}\frac{\partial \overline{\psi}}{\partial z} - \frac{\partial \overline{w'\psi'\psi'}}{\partial z} - 2\epsilon_\psi, \tag{22}$$

and found that for a dry convective boundary layer these two budgets were very similar. As another example, we show the variance budgets for the liquid water potential temperature variance ($\overline{\theta_l'^2}$) for the BOMEX cumulus case in Figure 1. It is clear that the bulk features of the two variance budgets are nearly the same. An inspection of the variance production term immediately makes clear that the fundamental massflux relation on which the top-hat approximation is based is satisfied:

$$\overline{w'\psi'} \approx M_c(\psi_u - \psi_d). \tag{23}$$

Moreover, the main conclusion of De Roode et al. (2000) that parameterizing the dissipation term in the Reynolds variance budget is analogous to parameterizing E and D in the massflux equations is also supported by the budgets for cumulus clouds.

In the next two sections we will explore whether we can find similar analogies between the prognostic massflux equation and the vertical velocity variance

equation. From the LES output we have computed the latter as follows

$$\frac{\partial \overline{w'^2}}{\partial t} = 2\frac{g}{\theta_0}\overline{w'\theta'_v} - \frac{\partial \overline{w'^3}}{\partial z} - 2\overline{w'\frac{\partial \pi'}{\partial z}} - 2\overline{w'\frac{\partial \tau'_{3j}}{\partial x_j}}. \tag{24}$$

where the primes indicate perturbations of the resolved variables with respect to the horizontal slab-mean value. If one samples the vertical momentum equation which is solved by the LES model one obtains for the prognostic massflux equation

$$\begin{aligned}
&\sigma_s(1-\sigma_s)\left(\left[\frac{\partial w}{\partial t}\right]_s - \left[\frac{\partial w}{\partial t}\right]_e\right) = \frac{g}{\theta_0}\sigma_s(1-\sigma_s)(\theta_{v,s}-\theta_{v,e}) \\
&-\sigma_s(1-\sigma_s)\left(\left[\frac{\partial w^2}{\partial z}\right]_s - \left[\frac{\partial w^2}{\partial z}\right]_e\right) - \sigma_s(1-\sigma_s)\left(\left[\frac{\partial u_h w}{\partial x_h}\right]_s - \left[\frac{\partial u_h w}{\partial x_h}\right]_e\right) \\
&-\sigma_s(1-\sigma_s)\left(\left[\frac{\partial \pi}{\partial z}\right]_s - \left[\frac{\partial \pi}{\partial z}\right]_e\right) - \sigma_s(1-\sigma_s)\left(\left[\frac{\partial \tau_{3j}}{\partial z}\right]_s - \left[\frac{\partial \tau_{3j}}{\partial z}\right]_e\right).
\end{aligned} \tag{25}$$

Every term in Eq.(25) has been computed from the LES output fields. Table 2 compares the components of the prognostic vertical velocity variance, massflux equations and the budget for the sampled vertical velocity u_s.

4. The budgets of the vertical velocity variance and the massflux

a. Budgets

To illustrate the dynamics of shallow cumulus clouds the budget for the vertical velocity variance $\overline{w'^2}$, computed according to (24), is shown in Figure 3. The buoyancy flux is the primary production source of $\overline{w'^2}$. Except for a shallow layer

around the cloud base the buoyancy flux is positive from the surface up to the inversion layer. At the top of the mixed layer, where the buoyancy flux is negative, saturated air parcels can reach their level of free convection by the upward vertical momentum they have gained. At these levels the turbulence transport term is the major term that is producing vertical velocity variance. In addition, the pressure term gives a positive, albeit small contribution, near the cloud base as well. The turbulent transport term becomes positive above about 1100 m. In the bulk of the cloud layer the dissipation and the pressure gradient term act to destroy vertical velocity variance. The pressure term redistributes vertical momentum into the horizontal directions, whereas the dissipation of the resolved vertical motions produces subgrid scale turbulence motions.

The massflux budgets as computed according to Eq. (25) have similar features as the vertical velocity variance budget (see Figure 4). The buoyancy term in the cloud massflux budget (sampling criterion I_2 according to Table 1) has a negative value at the upper part of the cloud layer. By definition, the cloud core must have a positive buoyancy. Irrespective of the kind of decomposition applied, the advection term is an important production term for the convective massflux in the upper part of the cloud layer. The conditionally sampled horizontal advection of vertical velocity, which is the lateral exchange of massflux, acts to produce massflux at the lower part of the cloud layer and diminishes the massflux above. The role of the pressure and subgrid flux terms are similar to the ones in the vertical velocity variance budget in the sense that they both tend to destroy massflux. In

that respect the subgrid flux term is analogous to the dissipation term in the vertical velocity variance budget, and this result might be somewhat controversial. Scaling considerations lead to the conclusion that dissipation by molecular viscosity can be neglected for motions on scales typical for cumulus convection, and that it is only of importance at the largest wavenumbers of the velocity spectra, the Kolmogorov scales. The 'dissipation' in the massflux budget, however, arises from the subgrid parameterization term (20) where the flux is parameterized as the product of an eddy-viscosity times the local gradient. In the turbulent kinetic energy equation it is exactly this term that causes the dissipation (see Table 2). However, the amount of the resolved kinetic energy that is lost is not dissipated into heat, but acts as a production term in the prognostic equation for the subgrid TKE equation, and therefore the subgrid term can be interpreted as a mechanism to convert resolved motions into subgrid perturbations. Hence, in the massflux budgets the subgrid parameterization term removes vertical momentum from the sampled eddies to feed the turbulent motions of small-scale eddies which have sizes smaller than the grid size of the LES.

b. Entrainment and detrainment

Siebesma and Cuijpers (1995) computed the lateral entrainment and detrainment rates by a careful analysis of the budget equation for conserved variables,

$$\frac{\partial \sigma \psi_s}{\partial t} = -\frac{\partial M_c \psi_s}{\partial z} - \frac{\partial \sigma \overline{w' \psi'}^s}{\partial z} + E\psi_e - D\psi_s + \sigma S_{\psi,s}, \qquad (26)$$

where the source term included large-scale forcing terms. Likewise, we can express a similar equation for the conditionally sampled vertical velocity,

$$\frac{\partial \sigma w_s}{\partial t} = -\frac{\partial M_c w_s}{\partial z} - \frac{\partial \sigma \overline{w'w'}^s}{\partial z} + E_w w_e - D_w w_s + \sigma S_{w,s}. \tag{27}$$

Here the source function comprises the buoyancy and the pressure,

$$S_{w,s} = \frac{g}{\theta_0}(\theta_{v,s} - \theta_0) - \left[\frac{\partial \pi}{\partial z}\right]_s. \tag{28}$$

From a comparison of (27) with the budget equation for the sampled velocity (see Table 2) it follows that the total lateral exchange term is given by

$$E_w w_e - D_w w_s = -\sigma \left[\frac{\partial u_h w}{\partial x_h}\right]_s - \sigma \left[\frac{\partial \tau_{3j}}{\partial x_j}\right]_s - \sigma_s \left\{\frac{\partial w}{\partial t}\right\}_{b,s} - \sigma_s \left\{\frac{\partial w^2}{\partial z}\right\}_{b,s}. \tag{29}$$

where the last two terms are the boundary terms according to (9). Note that the lateral exchange according to (29) differs from the one defined in Table 2, which only involves the divergence of the horizontal flux of vertical momentum. Although the massflux hardly changes with time, $\frac{\partial M_c}{\partial t} \approx 0$, the massflux budget for the cloud core showed that the total tendency of the massflux according to (25) is positive. It implies that the time tendency of the massflux is predominantly due to the Leibniz boundary term as in (9). It means that some of the cloud parcels that are accelerated disappear from the cloud sample at the next computational time step by detrainment.

If we use the continuity equation (3) we can solve E_w and D_w from (29). The results for the cloud core are shown in Figure 5. The detrainment rate profile is

similar to the one found for conserved variables by Siebesma and Cuijpers (1995). The entrainment rate compares less well with their findings; in the massflux budget equation E_w is smaller and even becomes negative above 1000 m. For other sampling criteria we also find negative values for E_w. The net effect of the entrainment rate in the massflux budget equation is negligibly small since it must be multiplied with the vertical velocity in the environment. For cumulus clouds w_e is generally a very small negative number. The surrounding air of the cloud core is not necessarily descending, clear air. It is even quite likely that upward moving, but negatively buoyant parcels are entrained by the cloud core which might be the cause of the negative sign of E_w.

5. Thermodynamic characteristics of the conditionally sampled cumulus clouds

a. The conditionally sampled virtual potential temperature flux and vertical velocity variance

Siebesma and Cuijpers (1995) found that the vertical turbulent fluxes of q_t and θ_l were primarily determined by in-cloud turbulence. Figure 6 shows the conditionally sampled virtual potential temperature flux $\sigma_s[\overline{w'\theta'_v}]_s$ and vertical velocity variance $\sigma_s[\overline{w'^2}]_s$. The vertical flux of the virtual potential temperature is mainly determined by in-cloud turbulence. Turbulent vertical motions in the cloud and in the environment contribute nearly equally to the vertical velocity variance.

Since θ_v is not conserved when evaporation/condensation of liquid water occurs, it is questionable how well the massflux approximation (23) holds for this variable. In Figure 7 its validity is checked for both the virtual potential temperature and the vertical velocity variance. For the cloud core decomposition the virtual temperature flux in the massflux approach $M_c(\theta_{v,s}-\theta_{v,e})$ is only a fraction smaller than the Reynolds-averaged flux $\overline{w'\theta_v'}$, but the difference between the Reynolds-averaged and massflux approximation is larger for the cloud updraft and cloud decomposition. This can be explained by the fact that for the cloud core parcels with a negative virtual potential temperature perturbation are filtered out, whereas $\theta_{v,s}$ for the cloud/cloud updraft is lowered by the inclusion of such parcels. The vertical velocity variance is not very well represented by any of the applied cloud decompositions, either. This can be expected because most of the vertical velocity variance is found outside the clouds (see Figure 6b).

b. Evaporative cooling and the generation of downdrafts

Figure 8 shows the conditionally sampled area fraction, vertical velocity, the virtual potential temperature and the total water content for the cloud updraft and downdraft, and the cloud core. The cloud downdraft fraction is rather small throughout the whole cloud layer. However, as is shown in Figure 9, its fraction of the total cloud cover increases from about 4% at 600 m to more than 20% above 1200 m. The average minimum vertical velocity of the cloud downdrafts decreases with height to about -0.7 m/s at 1500 m, where the cloud downdrafts have a significantly

lower virtual potential temperature than the horizontal slab-mean value. At about 1500 m the virtual potential temperature difference between the cloud downdrafts and the horizontal slab mean is nearly -1 K. The absolute value of this number is more than a factor of two larger than the maximum difference for the cloud core, which is about +0.4 K, where it should be noted that a positive buoyancy excess is one of the criteria that defines the cloud core.

The role of mixing of dry, environmental air with cloudy air at either the lateral sides of the cloud or the cloud top has been suggested to be a major mechanism leading to cold downdrafts (Raymond and Blyth, 1986; Kain and Fritsch, 1990; Taylor and Baker, 1991; Jonas, 1990). These downdrafts have been observed both within and just outside the cloud. To evaluate the possible role of lateral mixing on the formation of cold downdrafts we have computed the minimum virtual potential temperature that can be obtained by mixing cloudy and environmental air. It must be noted that although we refer to lateral mixing in this case, the cloud ensemble includes clouds in all possible stages, such as growing clouds which may mix with dry air at their tops. For a mixed parcel which contains a mixture of cloudy and environmental air the value of an arbitrary conserved variable ψ_m is given by

$$\psi_m = \chi\psi_e + (1-\chi)\psi_s, \tag{30}$$

where $\chi = \frac{m_1}{m_1+m_2}$ is the mixing fraction, m_1 and m_2 are the masses of a parcel from the surrounding cloud environment and cloud, respectively. If dry air is gradually mixed with cloudy air some cooling will take place by evaporation of liquid water (Randall, 1980; Deardorff, 1980; Duynkerke, 1993). The effect of

evaporative cooling is depicted in Figure 10. It shows how the virtual potential temperature changes as a function of the mixing fraction χ for a cloud parcel at 1000 m which mixes with dry environmental air. For the critical mixing fraction χ_* the maximum amount of cooling is obtained when all the liquid water is just evaporated. In the absence of liquid water, the virtual potential temperature can be considered to be a conserved variable, and the effect of mixing on the mixed parcel is a linear function of χ as described by Eq. (30). Note that the mixing fraction for which the mixed parcel is just neutrally buoyant is even smaller than the critical mixing fraction, and is about $\chi \approx 0.1$ for the example shown. Figure 11 shows the critical mixing fractions and the associated minimum virtual potential temperatures as a function of height for the cloud and cloud core decomposition. Less than 50% of dry air is needed to evaporate all the cloud core liquid water. The critical mixing fraction has a slightly smaller value for the cloud-environment decomposition since the mean sampled cloud liquid water content is lower than for the cloud core. However, irrespective the kind of cloud decomposition made, the minimum virtual potential temperature that can be obtained by lateral mixing is approximately the same. Furthermore, the minimum virtual potential temperature has a negative value at every height in the cloud layer. This can be easily explained by the fact that cloudy air has its primary origin in the subcloud layer which has a lower virtual potential temperature $\theta_{v,subcloud}$ than the cloud layer $\overline{\theta_v}(z)$. For example, Figure 11b also shows the virtual potential temperature difference between a dry undiluted parcel starting off from cloud base (z=500m) and the mean lapse

rate. After mixing between air from the subcloud and the conditionally unstable layer the virtual potential temperature of a just unsaturated mixed parcel ($\theta_{v,m}$) is constrained by

$$\theta_{v,subcloud} < \theta_{v,m} < \overline{\theta_v}(z). \tag{31}$$

In other words, Eq. (31) states that any unsaturated, mixed air parcel that has been detrained from the cloud will have a smaller virtual potential temperature with respect to the horizontal slab mean. It means that lateral mixing counteracts the latent heat release in the cumulus cloud and even causes the generation of cold air parcels that can sink and subsequently generate turbulent kinetic energy in the dry environment of the cumuli.

Note that if the mean virtual potential temperature of the cloud is less than in the environment it is likely that this is also the case for the temperature. It implies that if one measures a lower average temperature in a cumulus cloud from an instrumented aircraft this may be due to mixing and does not necessarily mean that the instrument is affected by wetting and a subsequent evaporative cooling.

Summarizing, the results presented in this section suggest that the top-hat approach for the vertical velocity tendency equation does not work as satisfactorily as for a conserved variable. The reason why this is the case is possibly best illustrated by Figure 8. If one compares the conditionally sampled total water contents for different criteria it is clear that they differ slightly, but nevertheless they all differ systematically from the environment. Because q_t is a conserved variable, mixing causes q_t to change according to (30) and as depicted by the linear mixing line in

Figure 10. The sign of the difference $(q_{t,s} - q_{t,e})$ is therefore conserved. However, this is not the case for the virtual potential temperature θ_v. Figure 10 shows that even for a small mixing fraction, $(\theta_{v,s} - \theta_{v,e})$ becomes negative. Since the buoyancy is the primary forcing term for the vertical velocity tendency, a negative buoyancy will cause the cloud updrafts to slow down and to become either cloud or dry negatively buoyant downdrafts.

6. Summary and conclusions

The dynamics of shallow cumulus have been investigated by means of a large-eddy simulation. By conditionally sampling on the presence of liquid water as an indicator function a distinction between clouds and environment could be made, while additional sampling criteria were used to select cloud downdrafts, cloud updrafts, and cloud cores (a positive vertical velocity and buoyancy excess).

A prognostic equation for the vertical massflux was derived by conditionally sampling the prognostic vertical velocity equation. The massflux budget was computed from a Large-Eddy Simulation based on the BOMEX observations and was compared with the vertical velocity variance budget. Qualitatively, these budgets have very similar features. The vertical velocity variance and the massflux are primarily driven by a positive buoyancy due to condensational heating in the cloud. In the upper part of cloud layer advection of vertical velocity becomes an important source for redistributing vertical velocity from the lower cloud layer. Pressure effects and the subgrid parameterization term are both acting to destroy the mass-

flux. The pressure redistributes vertical velocity into horizontal directions, while the subgrid term removes momentum from the resolved flow to feed turbulent subgrid eddies which have typical length scales that are smaller than the grid size of the LES model. Despite the fact that the budgets for different sampling criteria seem very similar by the eye, they are not identical. This means that, for example, if one develops a parameterization for the pressure term to be used in a prognostic massflux equation, the precise formulation of it depends on the particular definition one uses for the cloud.

Whereas the classical view sketches a cumulus cloud as a turbulent updraft surrounded by laminar compensating subsidence motions, a somewhat more complicated picture emerges from the LES results. First of all, the vertical velocity variance, which is a typical indicator of the turbulence intensity, is about as large in the cloud as in the dry environment. Possibly, a good deal of the vertical velocity variance in the dry environment can be attributed to gravity waves, which can develop owing to the conditionally unstable stratification in the cloud layer. The effect of turbulent motions in the cloud environment on the vertical transport of quantities like total water or the liquid water potential temperature is, however, very small.

Cloud downdrafts were found to occupy up to about 20% of the total cloud cover in the upper part of the cloud. Because the cloud downdrafts have a negative virtual potential temperature with respect to the horizontal slab mean this suggests that they were formed by mixing with dry environmental air giving rise to evapo-

rative cooling. The occurence of downdrafts and negatively buoyant parcels in the cloud has an important implication for massflux modeling. Whereas the vertical flux of a generic conserved variable ψ is well described by the massflux approach, it gives less satisfactory results for the virtual potential temperature and vertical velocity.

Acknowledgement This work was supported by NASA grant NAG1-2072. We thank Herve Greniew for the many stimulating discussions and Peter Duynkerke for giving useful comments on an earlier version of the manuscript.

References

Arakawa, A. and W. H. Schubert, 1974: Interaction of a cumulus cloud ensemble with the large-scale environment: Part i. *J. Atmos. Sci.*, **31**, 674–701.

Asai, T. and A. Kasahara, 1967: A theoretical study of the compensating downward motions associated with cumulus clouds. *J. Atmos. Sci.*, **24**, 487–496.

Cotton, W. R., 1975: On the parameterization of turbulent transport in cumulus clouds. *J. Atmos. Sci.*, **32**, 548–564.

Cuijpers, J. W. M., 1994: *Large-eddy simulation of cumulus convection*. Ph.D. thesis, Technical University Delft, Delft, 150 pp (Available from Technical University Delft, Delft, The Netherlands).

De Roode, S. R., P. G. Duynkerke, and A. P. Siebesma, 2000: Analogies between mass-flux and reynolds-averaged equations. *J. Atmos. Sci.*, **57**, 1585–1598.

Deardorff, J. W., 1973: Three-dimensional numerical modeling of the planetary boundary layer. *Workshop on Micrometeorology*, D. A. Haugen, ed., Amer. Met. Soc. Boston, 271–311.

— 1980: Cloud-top entrainment instability. *J. Atmos. Sci.*, **37**, 131–147.

Duynkerke, P. G., 1993: The stability of cloud top with regard to entrainment: Amendment of the theory of cloud-top entrainment instability. *J. Atmos. Sci.*, **50**, 495–502.

Grant, A. L. M. and A. R. Brown, 1999: A similarity hypothesis for shallow-cumulus transports. *Quart. J. Roy. Meteor. Soc.*, **125**, 1913–1936.

Holton, J. R., 1973: A one-dimensional cumulus model including pressure perturbations. *Mon. Wea. Rev.*, **101**, 201–205.

Jonas, P. R., 1990: Observations of cumulus cloud entrainment. *Atm. Res.*, **25**, 105–127.

Kain, J. S. and J. M. Fritsch, 1990: A one-dimensional entraining/detraining plume model and its application in convective parameterization. *J. Atmos. Sci.*, **47**, 2784–2802.

Nitta, T., 1975: Observational determination of cloud mass flux distributions. *J. Atmos. Sci.*, **32**, 73–91.

Raga, G. B., J. B. Jensen, and M. B. Baker, 1990: Characteristics of cumulus band clouds off the coast of hawaii. *J. Atmos. Sci.*, **47**, 338–355.

Randall, D. A., 1980: Conditional instability of the first kind upside down. *J. Atmos. Sci.*, **37**, 125–130.

Raymond, D. J. and A. M. Blyth, 1986: A stochastic mixing model for nonprecipitating cumulus clouds. *J. Atmos. Sci.*, **43**, 2708–2718.

Schumann, U. and C.-H. Moeng, 1991: Plume fluxes in clear and cloudy convective boundary layers. *J. Atmos. Sci.*, **48**, 1746–1757.

Siebesma, A. P. and Co-Authors, 2001: An intercomparison study for cloud resolving models of shallow cumulus convection. *Bull. Amer. Meteor. Soc.*, submitted.

Siebesma, A. P. and J. W. M. Cuijpers, 1995: Evaluation of parametric assumptions for shallow cumulus convection. *J. Atmos. Sci.*, **52**, 650–666.

Siebesma, A. P. and A. A. M. Holtslag, 1996: Model impacts of entrainment and detrainment rates in shallow cumulus convection. *J. Atmos. Sci.*, **53**, 2354–2364.

Stevens, B. and Co-Authors, 2000: Trade-wind cumuli under a strong inversion. *J. Atmos. Sci.*, submitted.

Stommel, H., 1947: Entrainment of air into a cumulus cloud. *J. Meteor.*, **4**, 91–94.

Taylor, G. R. and M. B. Baker, 1991: Entrainment and detrainment in cumulus clouds. *J. Atmos. Sci.*, **48**, 112–121.

Tiedtke, M., 1989: A comprehensive mass flux scheme for cumulus parameterization in large-scale models. *Mon. Wea. Rev.*, **177**, 1779–1800.

VanZanten, M. C., 2000: *Entrainment processes in stratocumulus*. Ph.D. thesis, Utrecht University, Utrecht, 139 pp (Available from Utrecht University, Utrecht, The Netherlands).

Young, G. S., 1988: Turbulence structure of the convective boundary layer. part iii: The vertical velocity budgets of thermals and their environment. *J. Atmos. Sci.*, **45**, 2039–2049.

Figure captions

Figure 1. The variance budgets for the liquid water potential temperature. (a) Reynolds-averaged equations. (b) Massflux equations for the cloud-environment decomposition. Linestyles are according to the legend shown in Figure 1a

Figure 2. (a) The mean virtual potential and (b) the mean liquid water content after 2 hours of simulation as a function of height. The results represent a 10 minute average.

Figure 3. The vertical velocity variance budget. Linestyles are according to the legend.

Figure 4. Massflux budgets. The linestyles are according to the legend shown in 4a.

Figure 5. Lateral entrainment (E_w) and detrainment (D_w) rates for the cloud core.

Figure 6. Sampled (a) virtual potential temperature flux ($\sigma_s[\overline{w'\theta'_v}]_s$) and (b) vertical velocity variance ($\sigma_s[\overline{w'^2}]_s$). Note that only the resolved part of the fluxes and variances have been sampled. The total resolved slab-averaged values of $\overline{w'\theta'_v}$ and $\overline{w'^2}$ are also shown for reference (solid lines). The linestyles are according to the legend shown in 6a.

Figure 7. (a) Virtual potential temperature flux, $M_c(\theta_{v,s}-\theta_{v,0})$, and (b) vertical velocity variance, $M_c(\theta_{v,s}-\theta_{v,0})$, in the massflux approach. The total resolved slab-averaged values (solid lines) are also shown for reference.

Figure 8. Conditionally sampling results. (a) The sampled area fraction σ_s. (b)

The vertical velocity w_s. (c) The virtual potential temperature excess relative to the horizontal mean value. (d) The total water content excess relative to the horizontal mean value. The profiles are representing a 4-hour averaged value. The linestyles are according to the legend shown in 8a.

Figure 9. The ratio of the cloud downdraft area fraction and the total cloud area fraction as a function of height.

Figure 10. Example of a mixing diagram showing how the virtual potential temperature depends on the mixing fraction between cloudy and dry environmental air. The diagram is computed from data at 1020 m for the cloud-environment decomposition.

Figure 11. (a) The critical mixing fraction χ_* as function of height. (b) The minimum virtual potential temperature excess with respect to the horizontal-slab mean that can be obtained after mixing of cloudy and environmental air and the virtual potential temperature difference between the cloud downdrafts and horizontal slab-mean value. Also shown is the difference of the virtual potential temperature of a rising undiluted, dry air parcel starting from z=500 m (dry-adiabatic ascent) and the horizontal slab-mean value. The linestyles are according to the legend.

Indicator function	Type	Sampling criteria
I_0	Slab mean	None
I_1	Updraft	$w > 0$
I_2	Cloud	$q_l > 0$
I_3	Cloud updraft	$q_l > 0$ and $w > 0$
I_4	Cloud downdraft	$q_l > 0$ and $w < 0$
I_5	Cloud core	$q_l > 0$ and $w > 0$ and $\theta_v > \overline{\theta_v}$

Table 1: **Summary of sampling criteria. $\overline{\theta_v}$ is the horizontal mean value of the virtual potential temperature and q_l is the liquid water content.**

	$\overline{w'^2}$	M_c budget	w_s budget
Tendency	$\frac{\partial \overline{w'^2}}{\partial t}$	$\frac{\partial M_c}{\partial t} + \sigma_s(1-\sigma_s)\left(\left\{\frac{\partial w}{\partial t}\right\}_{b,s} - \left\{\frac{\partial w}{\partial t}\right\}_{b,e}\right)$	$\frac{\partial w_s}{\partial t} + \frac{w_s}{\sigma_s}\frac{\partial \sigma_s}{\partial t} + \{\frac{\partial w}{\partial t}\}_{b,s}$
Buoyancy	$2\frac{g}{\theta_0}\overline{w'\theta'_v}$	$\frac{g}{\theta_0}\sigma_s(1-\sigma_s)(\theta_{v,s} - \theta_{v,e})$	$\frac{g}{\theta_0}(\theta_{v,s} - \theta_{v,0})$
Pressure	$-2\overline{w'\frac{\partial \pi'}{\partial z}}$	$-\sigma_s(1-\sigma_s)\left(\left[\frac{\partial \pi}{\partial z}\right]_s - \left[\frac{\partial \pi}{\partial z}\right]_e\right)$	$-\left[\frac{\partial \pi}{\partial z}\right]_s$
Turbulent transport	$-\frac{\partial \overline{w'^3}}{\partial z}$	$-\sigma_s(1-\sigma_s)\left(\left[\frac{\partial w^2}{\partial z}\right]_s - \left[\frac{\partial w^2}{\partial z}\right]_e\right)$	$-\frac{\partial \left[w^2\right]_s}{\partial z} - \frac{\left[w^2\right]_s}{\sigma_s}\frac{\partial \sigma_s}{\partial z} - \{\frac{\partial w^2}{\partial z}\}_{b,s}$
Dissipation	$-2\overline{w'\frac{\partial \tau'_{3j}}{\partial x_j}}$	$-\sigma_s(1-\sigma_s)\left(\left[\frac{\partial \tau_{3j}}{\partial z}\right]_s - \left[\frac{\partial \tau_{3j}}{\partial z}\right]_e\right)$	$-\left[\frac{\partial \tau_{3j}}{\partial z}\right]_s$
Shear production/lateral exchange	$-2\overline{u'_h w'}\frac{\overline{U}_h}{\partial z}$	$-\sigma_s(1-\sigma_s)\left(\left[\frac{\partial u_h w}{\partial z}\right]_s - \left[\frac{\partial u_h w}{\partial z}\right]_e\right)$	$-\left[\frac{\partial u_h w}{\partial z}\right]_s$

Table 2: **Summary of the terms in the vertical velocity variance, massflux, and conditionally sampled vertical velocity budgets.**

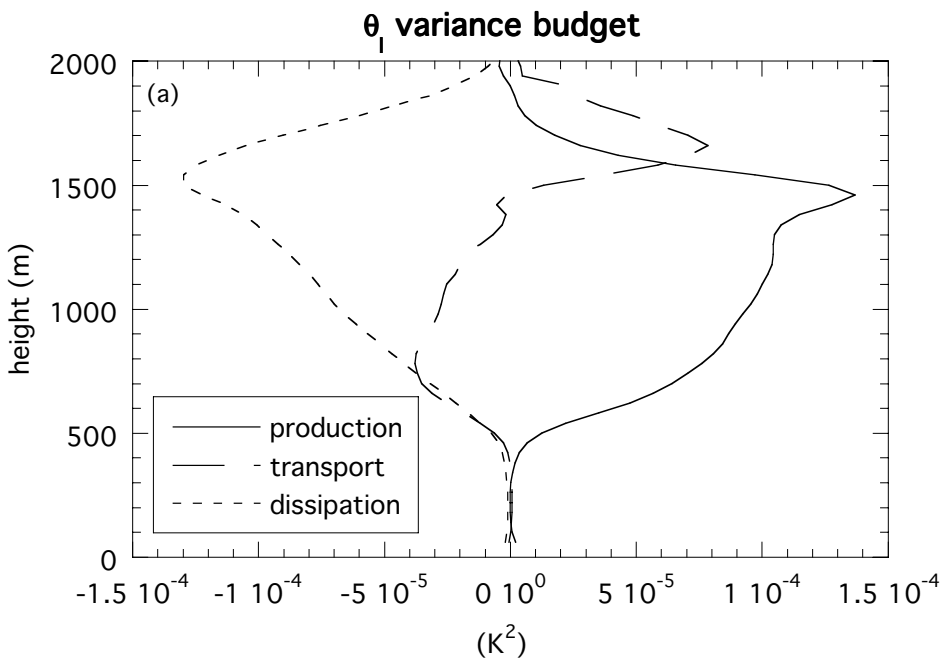
θl variance budget
(a)
height (m)
2000
1500
1000
500
0
production
transport
dissipation
-1.5 10-4
-1 10-4
-5 10-5
0 100
5 10-5
1 10-4
1.5 10-4
(K2)

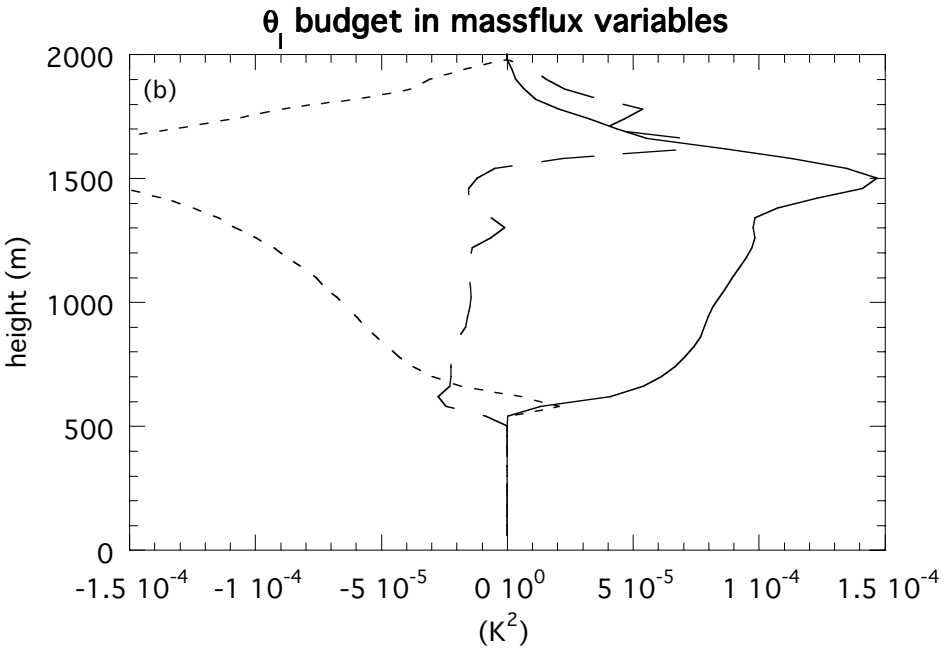
θl budget in massflux variables
(b)
height (m)
2000
1500
1000
500
0
-1.5 10-4
-1 10-4
-5 10-5
0 100
5 10-5
1 10-4
1.5 10-4
(K2)

Figure 1:

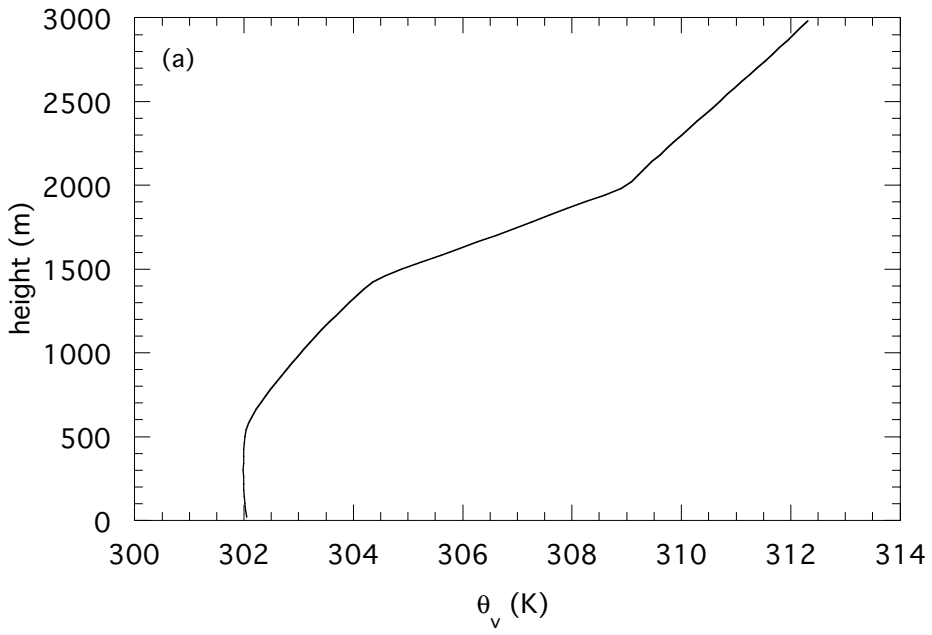
(a)
height (m)
3000
2500
2000
1500
1000
500
0
300
302
304
306
308
310
312
314
θv (K)

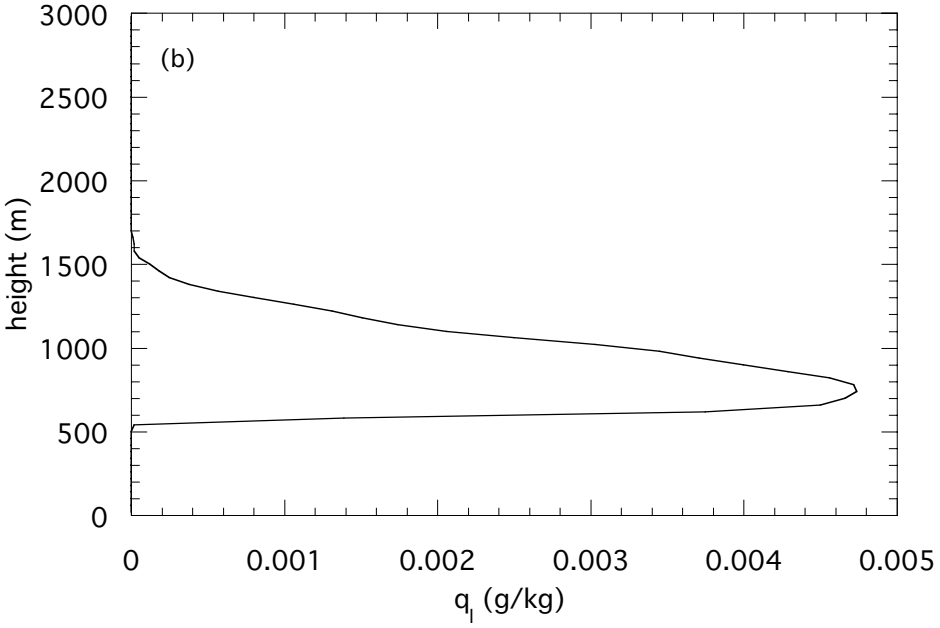
(b)
height (m)
3000
2500
2000
1500
1000
500
0
0
0.001
0.002
0.003
0.004
0.005
ql (g/kg)

Figure 2:

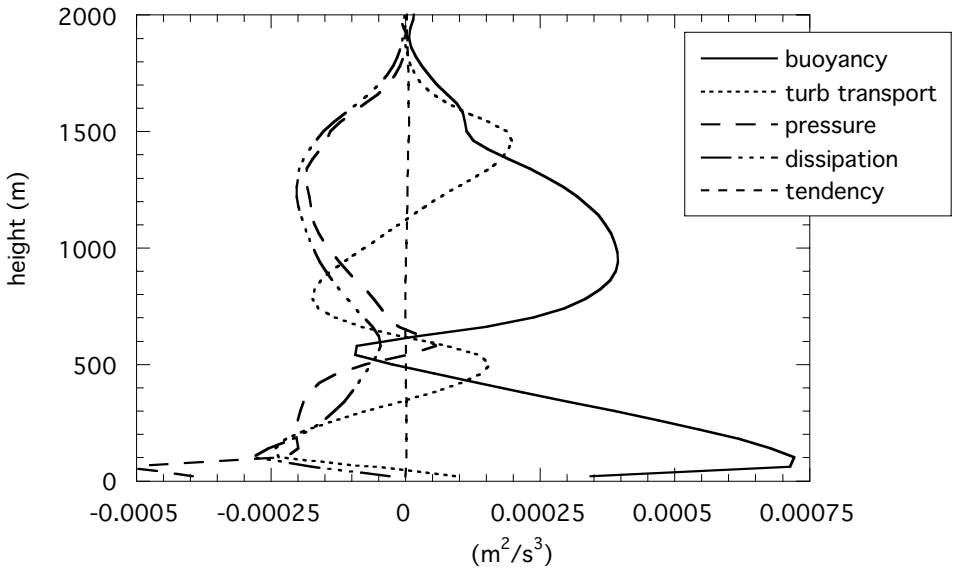
2000
1500
1000
500
0
height (m)
-0.0005
-0.00025
0
0.00025
0.0005
0.00075
(m²/s³)
buoyancy
turb transport
pressure
dissipation
tendency

Figure 3:

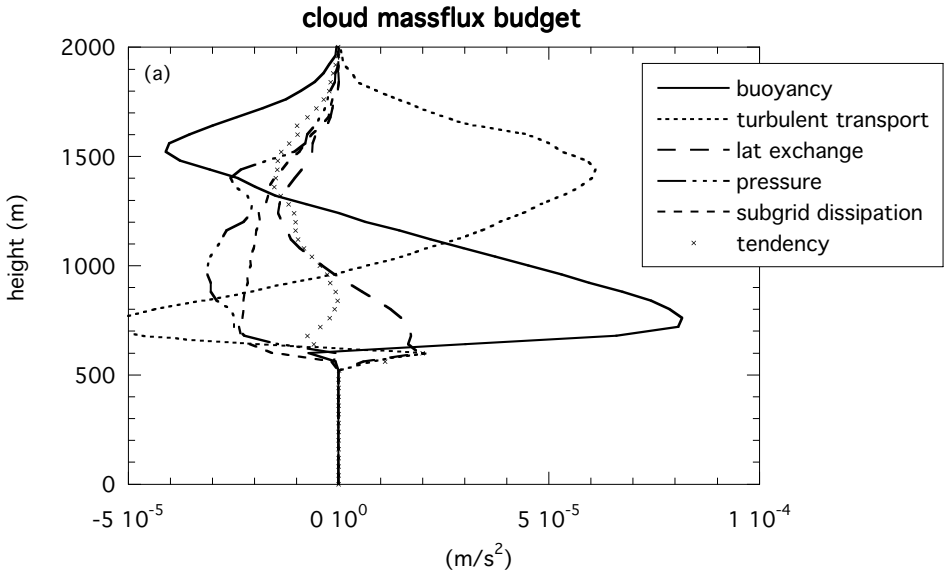
cloud massflux budget
(a)
buoyancy
turbulent transport
lat exchange
pressure
subgrid dissipation
tendency
height (m)
2000
1500
1000
500
0
-5 10^-5
0 10^0
5 10^-5
1 10^-4
(m/s^2)

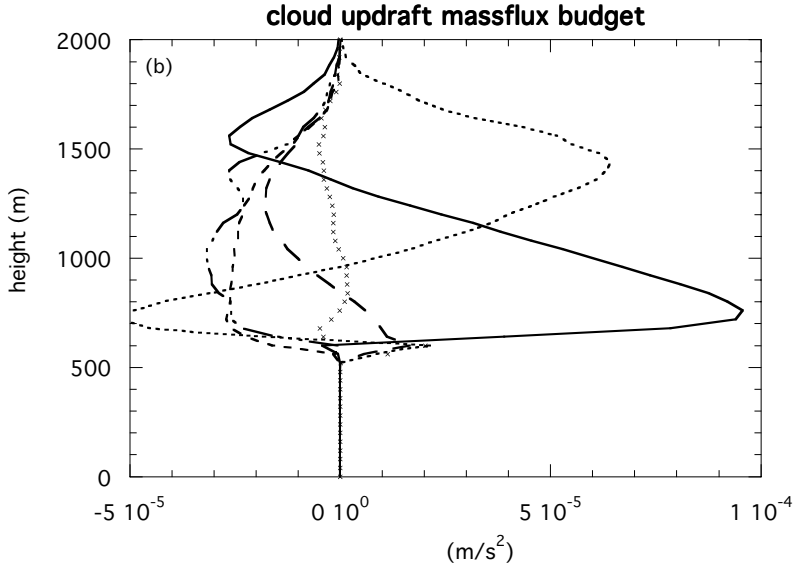
cloud updraft massflux budget
(b)
height (m)
2000
1500
1000
500
0
-5 10^-5
0 10^0
5 10^-5
1 10^-4
(m/s^2)

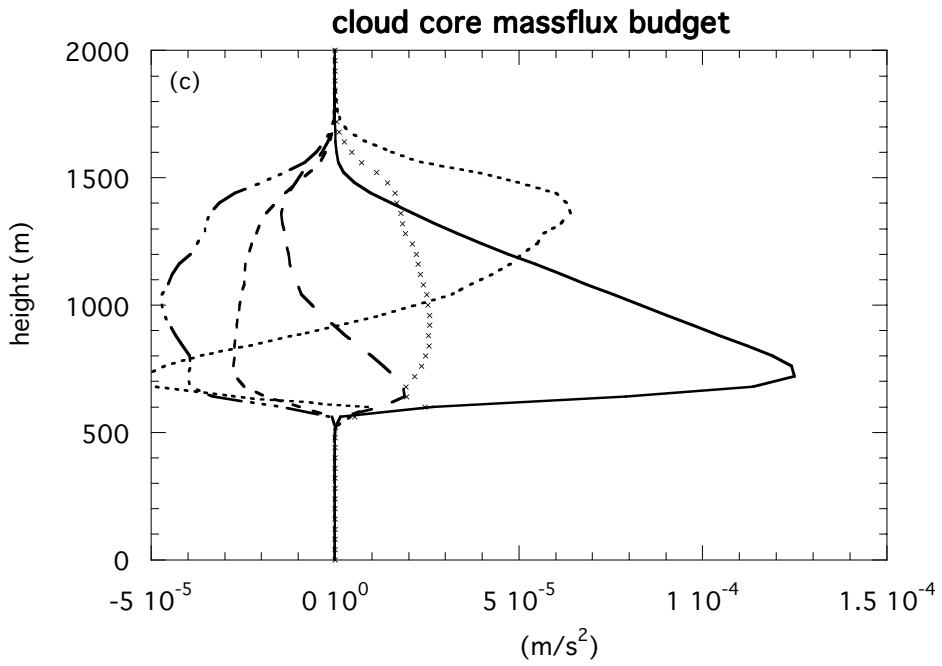
cloud core massflux budget
(c)
height (m)
2000
1500
1000
500
0
-5 10^-5
0 10^0
5 10^-5
1 10^-4
1.5 10^-4
(m/s^2)

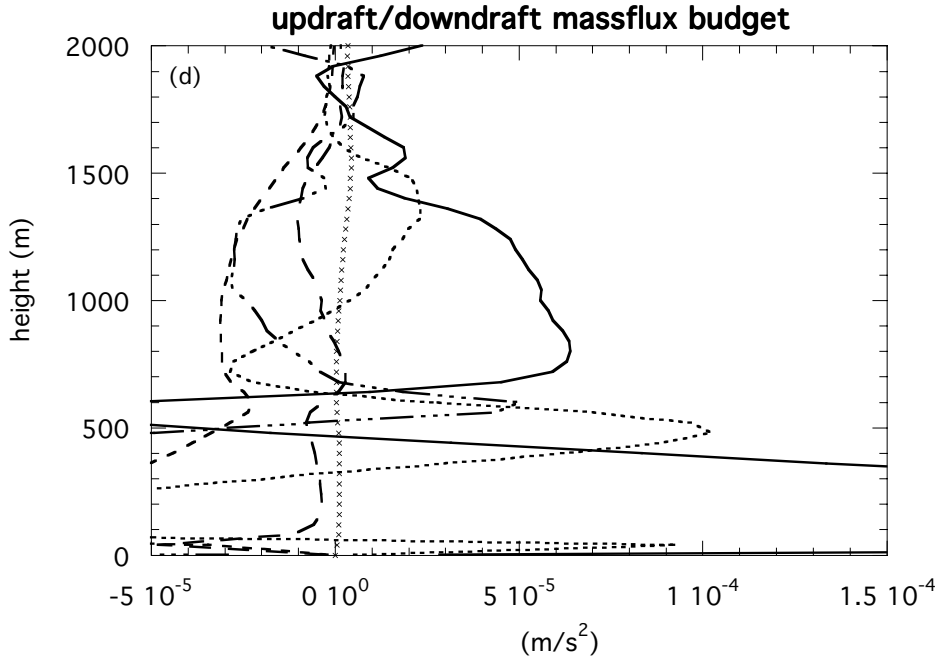
updraft/downdraft massflux budget
(d)
height (m)
2000
1500
1000
500
0
-5 10^-5
0 10^0
5 10^-5
1 10^-4
1.5 10^-4
(m/s^2)

Figure 4:

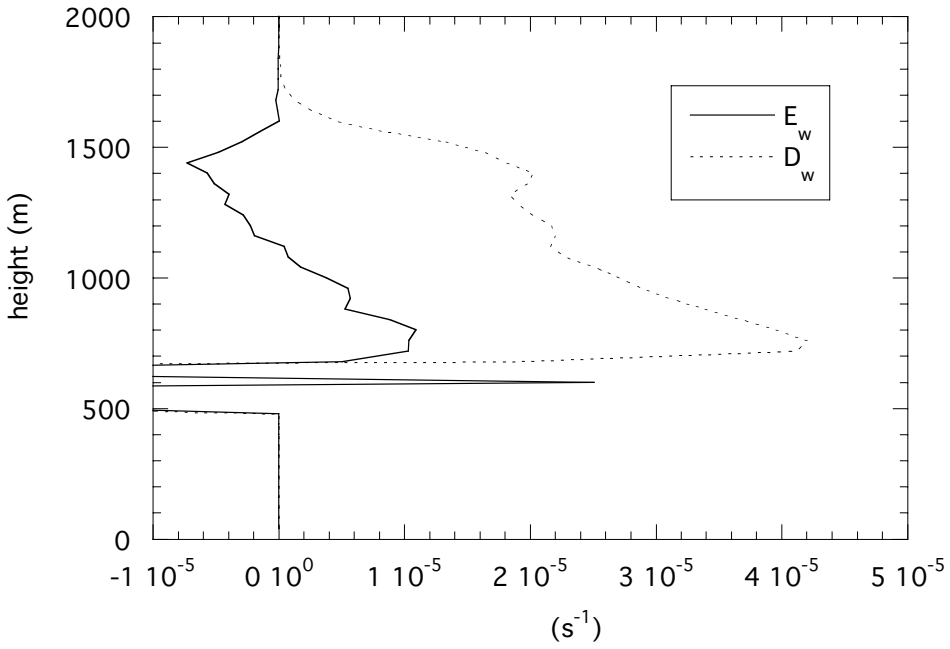
2000
1500
1000
500
0
height (m)
E w
D w
-1 10-5
0 100
1 10-5
2 10-5
3 10-5
4 10-5
5 10-5
(s-1)

Figure 5:

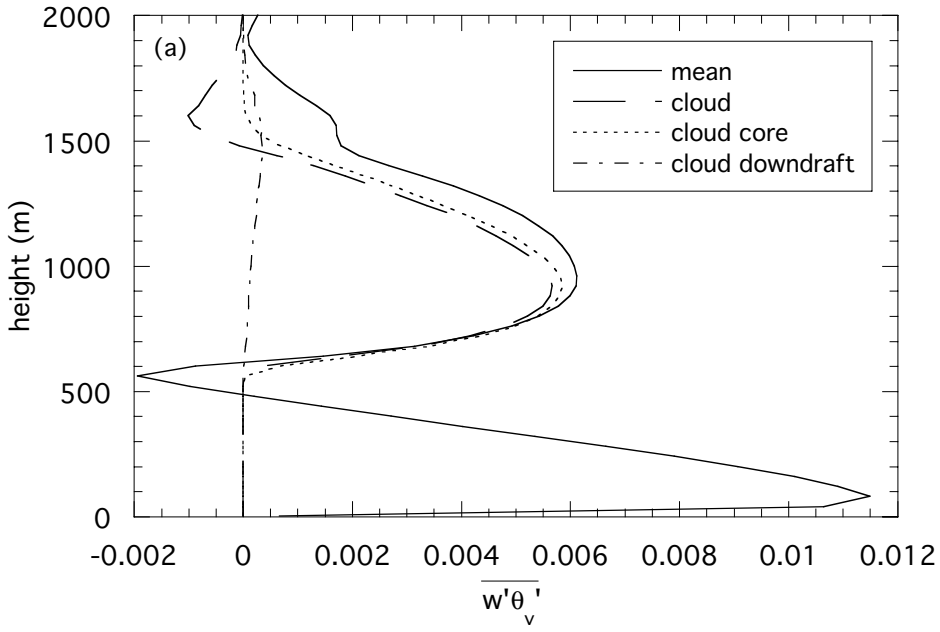
(a)
mean
cloud
cloud core
cloud downdraft
height (m)
2000
1500
1000
500
0
-0.002
0
0.002
0.004
0.006
0.008
0.01
0.012
$\overline{w'\theta_v'}$

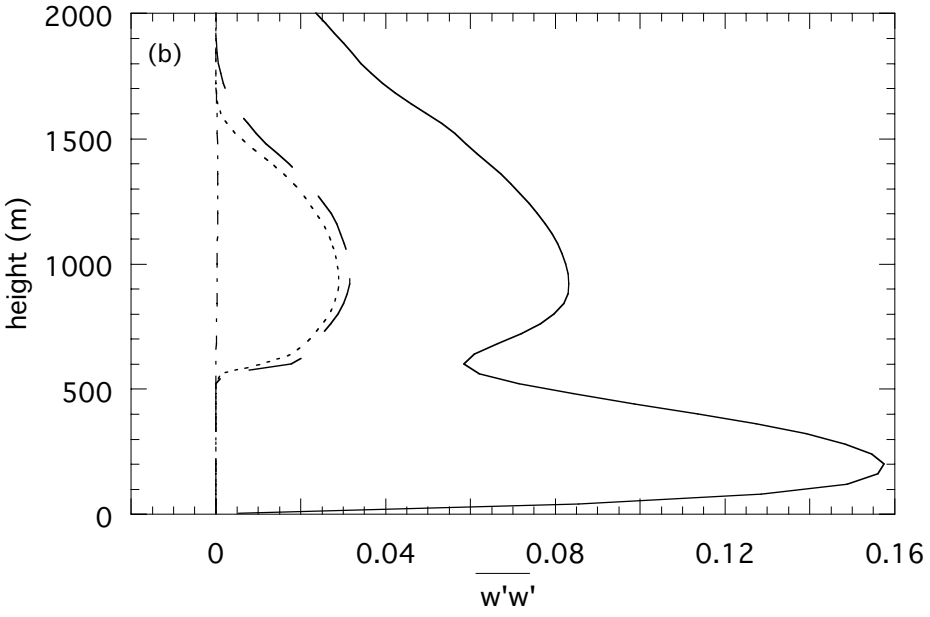
(b)
height (m)
2000
1500
1000
500
0
0
0.04
0.08
0.12
0.16
$\overline{w'w'}$

Figure 6:

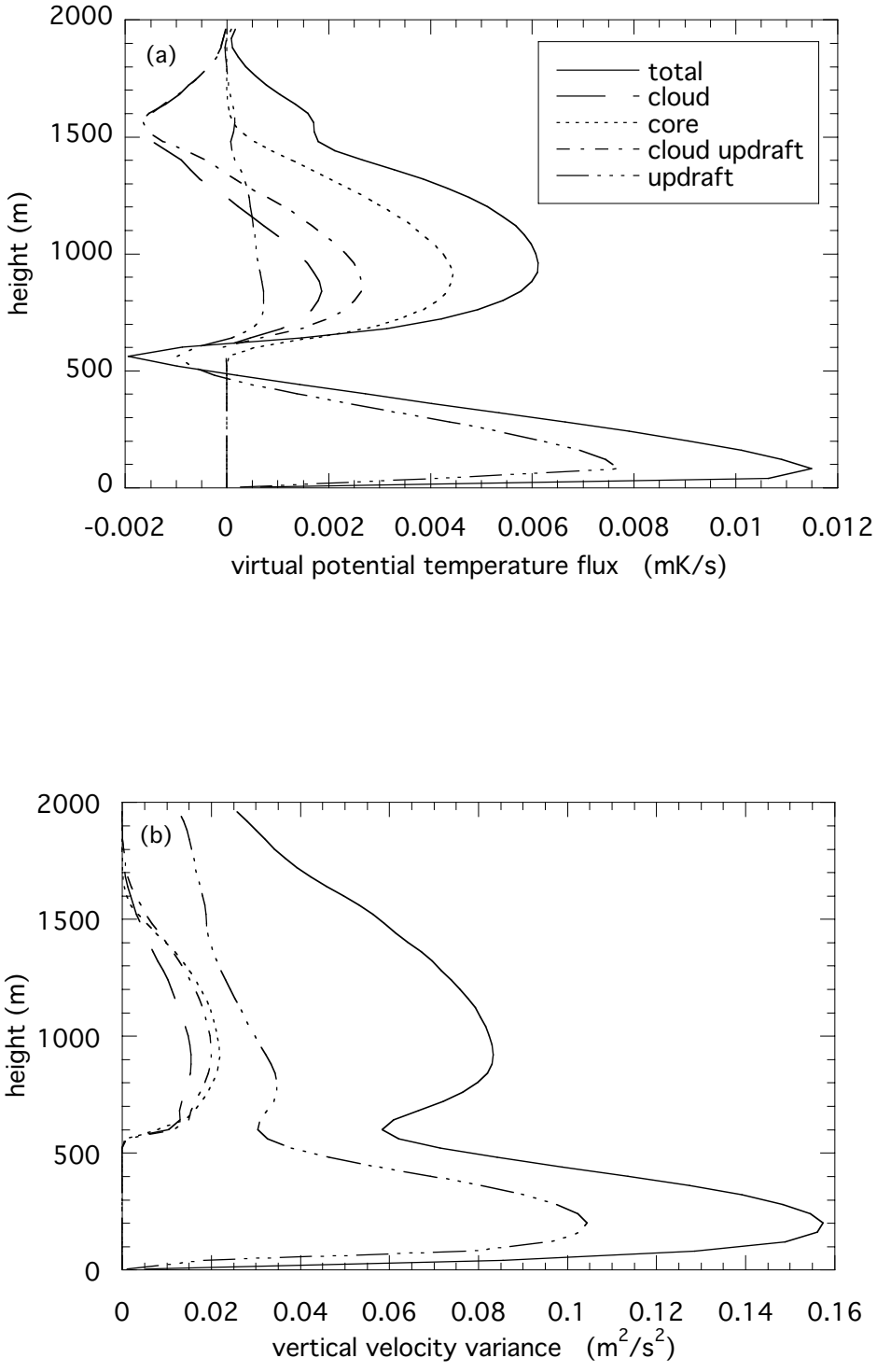
(a)
total
cloud
core
cloud updraft
updraft
height (m)
2000
1500
1000
500
0
-0.002
0
0.002
0.004
0.006
0.008
0.01
0.012
virtual potential temperature flux (mK/s)
(b)
height (m)
2000
1500
1000
500
0
0
0.02
0.04
0.06
0.08
0.1
0.12
0.14
0.16
vertical velocity variance (m^2/s^2)

Figure 7:

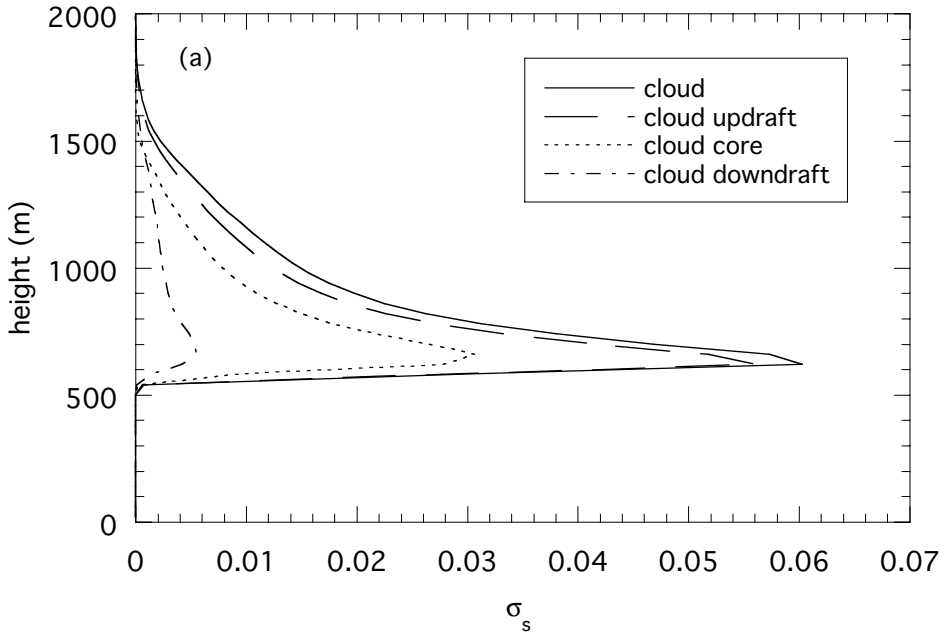
(a)
cloud
cloud updraft
cloud core
cloud downdraft
height (m)
2000
1500
1000
500
0
0
0.01
0.02
0.03
0.04
0.05
0.06
0.07
σs

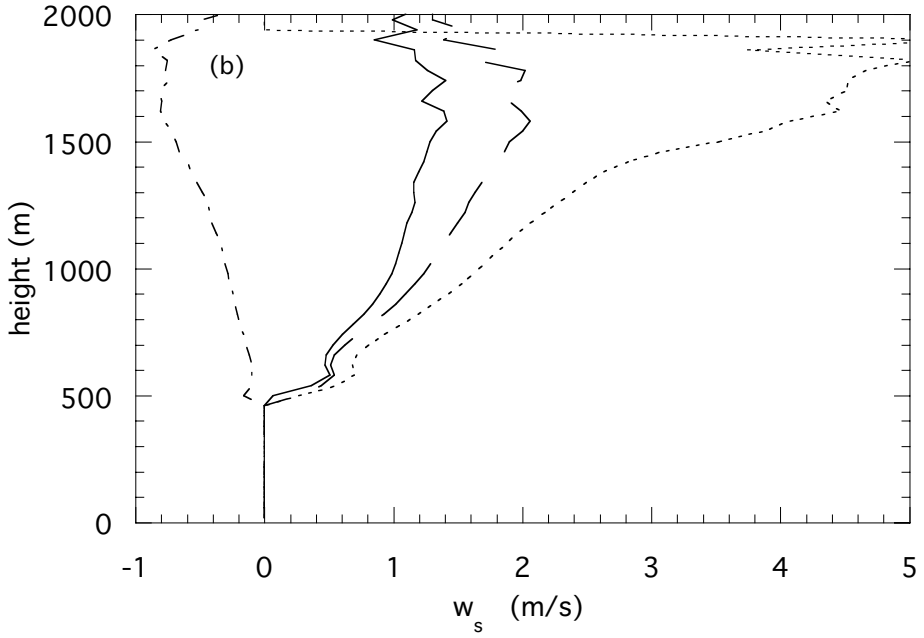
(b)
height (m)
2000
1500
1000
500
0
-1
0
1
2
3
4
5
ws (m/s)

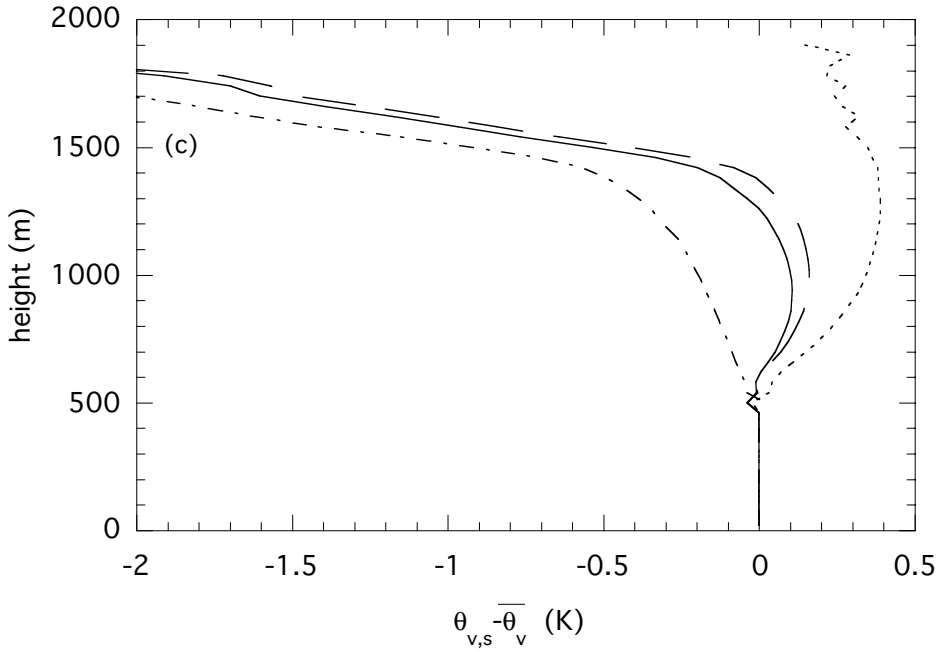
2000
1500
1000
500
0
height (m)
(c)
-2
-1.5
-1
-0.5
0
0.5
θv,s -θv (K)

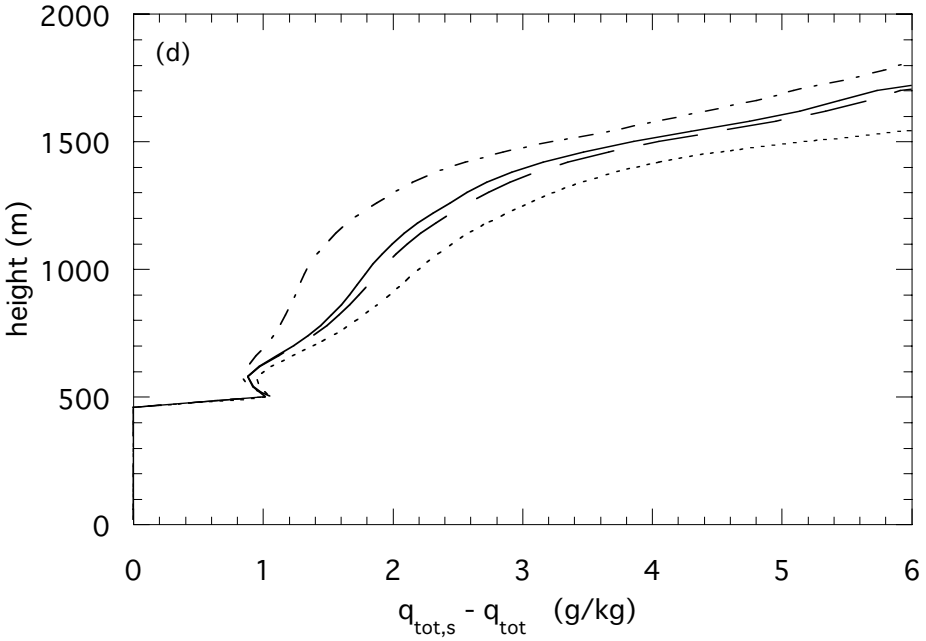
2000
1500
1000
500
0
height (m)
(d)
0
1
2
3
4
5
6
qtot,s - qtot (g/kg)

Figure 8:

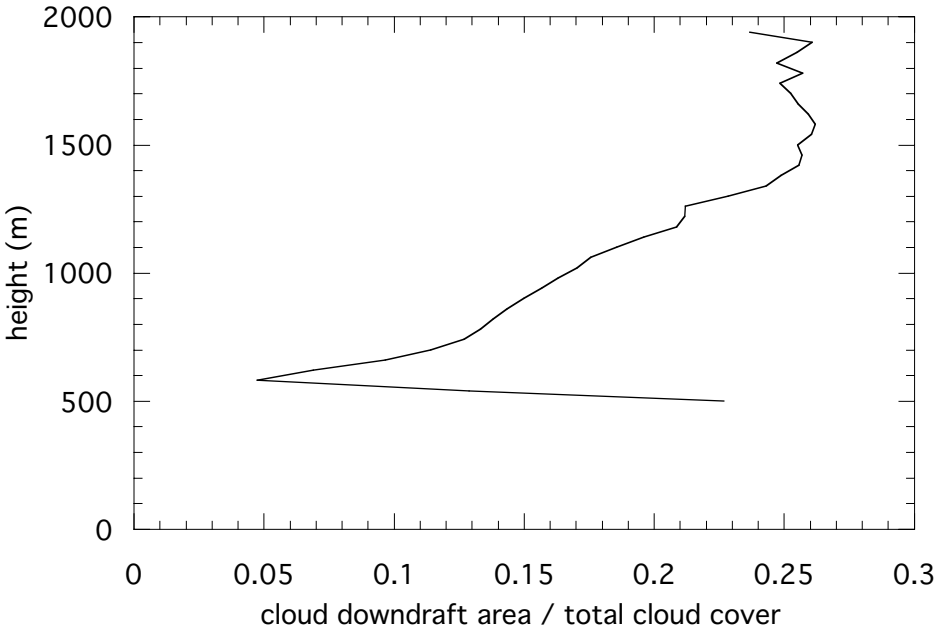
2000
1500
1000
500
0
height (m)
0
0.05
0.1
0.15
0.2
0.25
0.3
cloud downdraft area / total cloud cover

Figure 9:

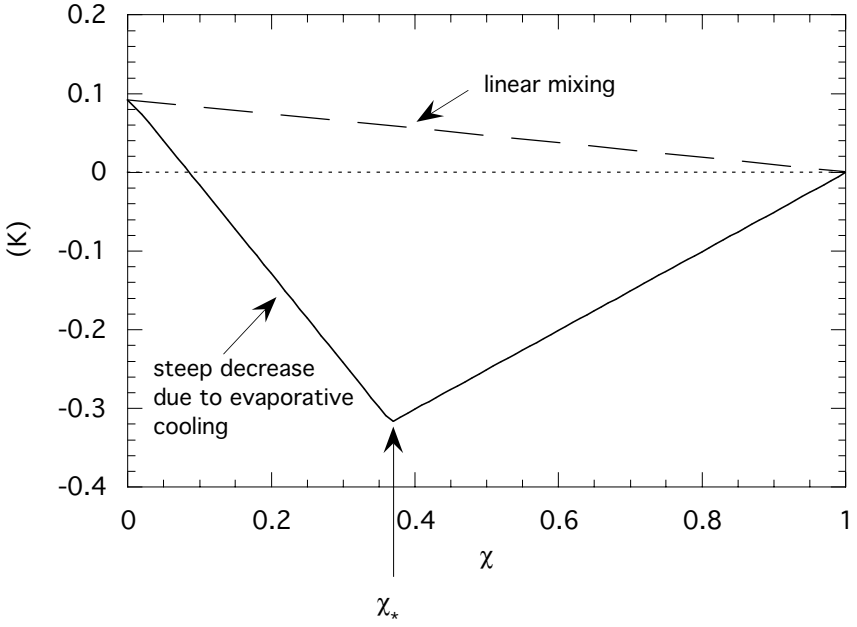
0.2
0.1
0
-0.1
-0.2
-0.3
-0.4
(K)
0
0.2
0.4
0.6
0.8
1
χ
χ*
linear mixing
steep decrease
due to evaporative
cooling

Figure 10:

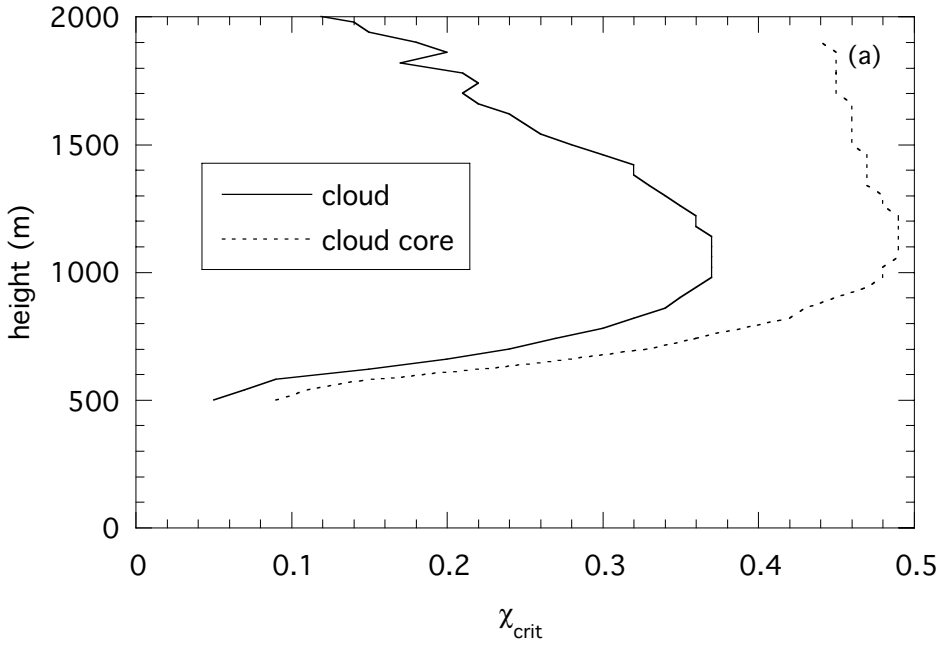
2000
1500
1000
500
0
height (m)
0
0.1
0.2
0.3
0.4
0.5
χcrit
(a)
cloud
cloud core

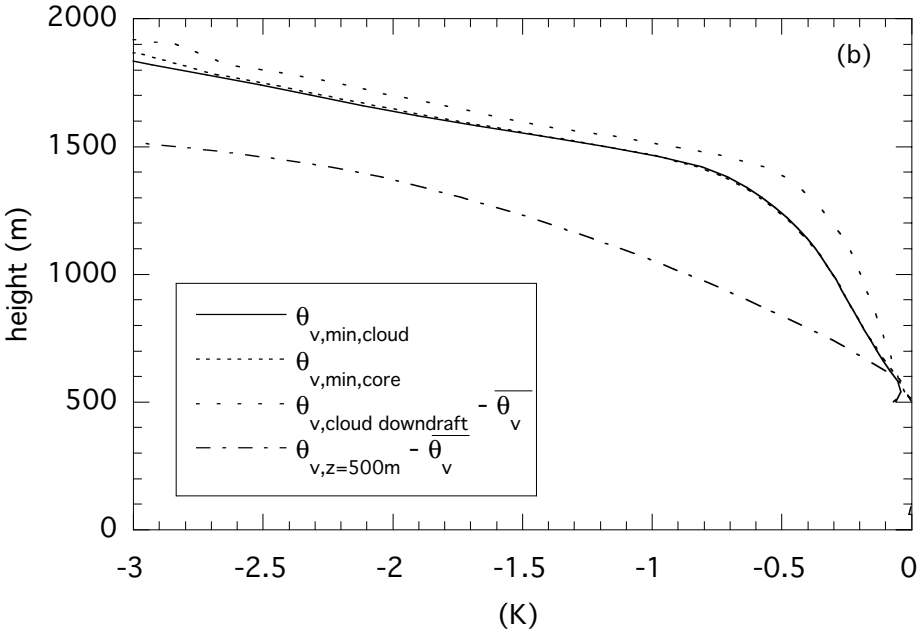
2000
1500
1000
500
0
height (m)
-3
-2.5
-2
-1.5
-1
-0.5
0
(K)
(b)
θv,min,cloud
θv,min,core
θv,cloud downdraft - θv
θv,z=500m - θv

Figure 11: